J Solid State Electrochem (2003) 7: 380–388
DOI 10.1007/s10008-002-0346-8

ORIGINAL PAPER

Jin-Ju Park · Su-Il Pyun

Analysis of impedance spectra of a pitted Inconel alloy 600 electrode in chloride ion-containing thiosulfate solution at temperatures of 298–573 K

Received: 28 August 2002 / Accepted: 10 November 2002 / Published online: 5 February 2003

Abstract In the present work, impedance spectra of a pitted Inconel alloy 600 electrode were analysed in aqueous 0.1 M $Na_2S_2O_3$ + 0.1 M NaCl solution at elevated solution temperatures of 298–573 K and at pressures of 0.1–8 MPa in terms of pit size distribution, fractal dimension and surface roughness in sequence as the solution temperature rose. From impedance spectra of the Nyquist plot obtained from the pitted specimen exposed to solutions at temperatures of 60–150°C, a constant phase element (CPE) was observed in the frequency range from 10^3 to 1 Hz. Especially, it was found that the impedance spectra were divided into two sections, i.e. a first CPE with a smaller slope in the higher frequency range and a second CPE with a larger slope in the lower frequency range. The occurrence of the two kinds of CPE results from a transition of ion diffusion through the pit to ion accumulation at the pit bottom, which is caused by double-layer charging at the pit bottom and prior double-layer charging at the pit wall. Impedance spectra were simulated in terms of pit size distribution and values of the fractal dimension of the pits as a function of solution temperature to compare with those spectra measured experimentally. The spectra were simulated based upon the conventional transmission line model for a cylindrically shaped pit at 60 °C and on the basis of a modified transmission line model for the triadic Koch construction at 100 °C and for the quadratic Koch construction at 150 °C. The modified transmission line model takes into account the resistive and capacitive elements in the lateral direction as well as those in the downward direction of the three-dimensional Koch constructions. Above 200 °C the Nyquist plots were found to be depressed more noticeably from a perfect semicircular form with increasing solution temperature. This is due to the increase in the surface roughness of the specimen by the formation and growth of the pits.

Keywords Constant phase element · Impedance spectroscopy · Inconel alloy 600 · Koch construction · Pit size distribution

J. Park · S.-I. Pyun (✉)
Department of Materials Science and Engineering,
Korea Advanced Institute of Science and Technology,
373-1 Guseong-dong, Yuseong-gu, 305-701,
Daejeon, Republic of Korea
E-mail: sipyun@mail.kaist.ac.kr
Tel.: +82-42-8693319
Fax: +82-42-8693310

Introduction

Inconel alloy 600 is used extensively in steam generator tubing in commercial pressurized water reactors. However, pitting attack has been observed in the steam generator tubes. Hence, a number of studies of pitting corrosion of alloy 600 tubes have been conducted in various steam generator environments [1, 2, 3]. In most cases, the measurement of the pitting potential and the results of the exposure tests were used to assess the pitting resistance of alloy 600 tubes in a given environment.

In recent years, fractal geometry has proved to be useful to describe irregularities in the morphology of corroded surfaces [4, 5, 6, 7]. Especially, pitting corrosion can lead to irregular rough surfaces because of the formation and decay of a protective layer. In this respect, in previous work [8] the relationship between the morphology of the pits formed on alloy 600 at various solution temperatures and the fractal dimension has been successfully established using scanning electron microscopy (SEM), electrochemical impedance spectroscopy and image analysis methods. In particular, the changes in the morphology and the fractal dimension value of the pits during the whole pitting process have been discussed with respect to solution temperature in terms of the degree of passivity of the oxide film. However, the occurrence of constant phase element (CPE) behaviour and depression in the impedance spectra of pitted alloy 600 electrodes at different solution

temperatures are not fully understood. Accordingly, it is necessary to analyse impedance spectra of alloy 600 in terms of pit size distribution, fractal dimension and surface roughness as a function of solution temperature.

The aim of the present work is to analyse impedance spectra of pitted Inconel alloy 600 electrodes in aqueous 0.1 M $Na_2S_2O_3$ + 0.1 M NaCl solution at elevated solution temperatures of 298–573 K and at pressures of 0.1–8 MPa. For this purpose, impedance spectra in solutions at 60–150 °C have been simulated in terms of pit size distribution and the fractal dimension value in sequence as the solution temperature rises. Subsequently, the calculated spectra have been compared with those spectra experimentally measured. Furthermore, the depression of the impedance plot above 200 °C has been discussed in terms of the change in surface roughness of the pitted electrode with respect to the solution temperature.

Experimental

The material used in this study was Inconel alloy 600 with a composition (wt%) of 15.4% Cr, 8.0% Fe, 0.3% Mn, 0.1% Si, 0.01% C and Ni (balance). For electrochemical experiments, a squared rod specimen was set in a block of polyimide and then mechanically polished with emery paper successively up to 2000 grit. As test solution, a mixed aqueous solution of 0.1 M $Na_2S_2O_3$ and 0.1 M NaCl at 25–300 °C under pressures of 0.1–8 MPa was employed. All electrochemical measurements at elevated solution temperatures and pressures were carried out using a home-made autoclave.

A platinum wire was used as the counter electrode and the potentials were measured and controlled with an external, cooled Ag/AgCl reference electrode prepared by filling the entire compartment with 0.1 M KCl solution. The external reference electrode consisted of an Ag/AgCl electrode housed in a stainless steel compartment that was maintained at ambient temperature. The reference electrode compartment was connected to the high-temperature autoclave by a high-pressure fitting. Working and counter electrodes were introduced into the autoclave through a high-pressure fitting.

AC impedance measurements were conducted with a Solartron 1255 Frequency Response Analyzer connected with a Solartron 1287 Electrochemical Interface. Two types of measurements were done. Firstly, in order to investigate the effect of pit morphology on impedance behaviour, the pitted electrode specimen was prepared by applying a potential of 0.8 $V_{Ag/AgCl}$ for 300 s in aqueous 0.1 M $Na_2S_2O_3$ + 0.1 M NaCl solution at various solution temperatures. Thereafter, impedance spectra were recorded on the previously pitted specimen under open circuit conditions at room temperature in 0.5 M Na_2SO_4 solution. Secondly, for the determination of the depression parameter, impedance spectra were measured on the pitted specimen in aqueous 0.1 M $Na_2S_2O_3$ + 0.1 M NaCl solution at various applied potentials and solution temperatures. Impedance spectra were recorded from 10^5 Hz down to 10^{-1} Hz frequency using 5 mV amplitude perturbation.

The pit morphology of the pitted specimen was examined as a function of solution temperature using SEM. Thereafter, the value of fractal dimension D_f of the pits was determined using the perimeter-area method [9, 10]. To calculate the perimeter-area dimension, it is necessary to measure the perimeter and the area of the pits with boxes of different yardsticks, and plot the logarithm of the pit perimeter on the vertical axis versus the logarithm of the pit area on the horizontal axis. If the relationship is indeed fractal, this plot will follow a straight line with a positive slope that equals $D_f/2$.

A PSI ProScan M5 (Park Scientific Instruments) atomic force microscope (AFM) was used to determine the change in the roughness parameter of several pitted specimens exposed to solutions at 200, 250 and 300 °C. The scan was made over an area of 70×70 μm^2 with a resolution of 256×256 pixels.

Results and discussion

Effect of pit morphology on impedance behaviour of alloy 600 in solutions at 60–150 °C

Figure 1a–c shows typical SEM micrographs of the pit morphology of the surface of the pitted specimen prepared at 60, 100 and 150 °C, respectively. It was observed that the morphology of the pits changed from a cylindrical shape at 60 °C to a highly branched shape at 150 °C. In addition, the value of the fractal dimension was determined from the pit morphology with the help of the perimeter-area method [9, 10]. As a result, as the solution temperature was raised the value of fractal dimension increased as follows: $D_f(60\ °C) = 1.04 \pm 0.04$, $D_f(100\ °C) = 1.24 \pm 0.06$ and $D_f(150\ °C) = 1.40 \pm 0.1$.

Figure 2 shows impedance spectra in Nyquist presentation obtained from the pitted specimens at open circuit potential in aqueous 0.5 M Na_2SO_4 solution at room temperature. In this figure, a CPE was observed in the frequency range from 10^3 to 1 Hz. At the same time, it was found that impedance spectra measured from the three kinds of pitted specimens were similar to one another in value and shape. In particular, it was found that impedance spectra containing a CPE were divided into two sections, i.e. a first CPE with a smaller slope in the frequency range from 10^3 to 10 Hz and a second CPE with a larger slope in the frequency range from 10 to 1 Hz. The first CPE shows ion diffusion through the pit, which is due to the combination of the resistive element of the solution and the capacitive element at the pit wall. Moreover, the second CPE represents ion accumulation at the pit bottom, which is attributable to double-layer charging at the pit bottom including prior double-layer charging at the pit wall.

In addition, one observed clearly the inclined lines of the first and second CPEs in the Nyquist plot, whose slopes were larger than 45° and smaller than 90°, respectively. This occurrence of the inclined line in the Nyquist plot is assumed to be due to pit size distribution, which is similar to the case of pore size distribution [11]. Therefore, in order to analyse impedance spectra containing a CPE, impedance spectra were simulated in terms of pit size distribution at 60, 100 and 150 °C and the fractal dimension value of the pits at 100 °C and 150 °C and the resulting simulated spectra were compared with those spectra experimentally measured (see below).

Analysis of impedance spectra of alloy 600 exposed to 60 °C solution based on the transmission line model

The transmission line model for a porous electrode was first introduced by de Levie [12, 13]. He considered that the impedance of a porous electrode could be described

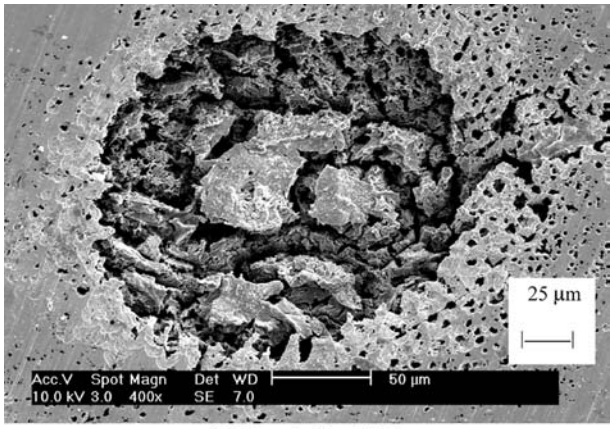

(a) $D_f = 1.04 \pm 0.04$

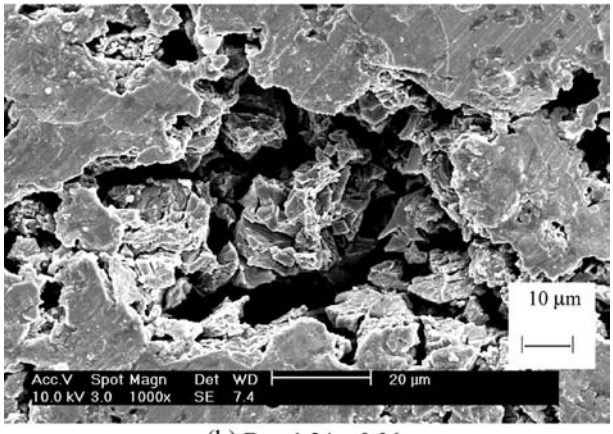

(b) $D_f = 1.24 \pm 0.06$

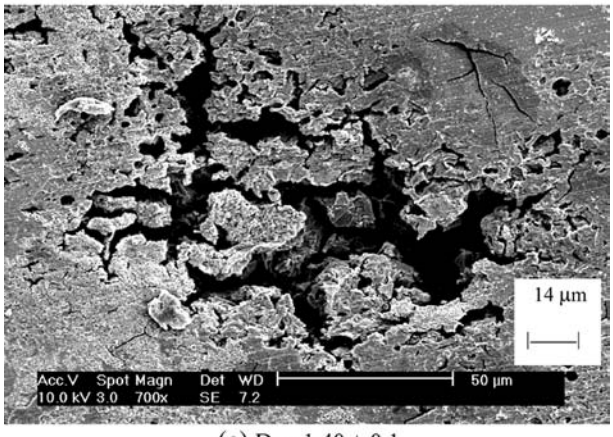

(c) $D_f = 1.40 \pm 0.1$

Fig. 1 Typical SEM micrographs of pit morphology on the surface of alloy 600 subjected to a constant anodic potential of 0.8 $V_{Ag/AgCI}$ for 300 s in aqueous 0.1 M $Na_2S_2O_3 + 0.1$ M NaCI solution at **a** 60 °C, **b** 100 °C and **c** 150 °C

by a parallel scheme of identical cylindrical pores. The impedance of a cylindrical pore was calculated by the transmission line technique. In the present work, the shape of a pit formed at 60 °C was cylindrical, as shown in Fig. 1a. Moreover, assuming that the pit size distribution is responsible for the occurrence of the inclined line in the Nyquist plot, we employed the transmission

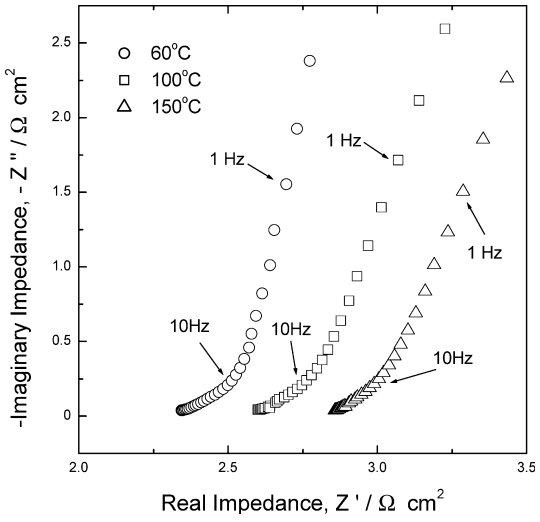

Fig. 2 Impedance spectra in Nyquist presentation obtained from alloy 600 at open circuit potential in aqueous 0.5 M Na_2SO4 solution at room temperature after anodic polarization of 0.8 $V_{Ag/AgCI}$ for 300 s in aqueous 0.1 M $Na_2S_2O_3 + 0.1$ M NaCI solution at various solution temperatures

line model [12, 13] to calculate the impedance spectra of cylindrically shaped pits at 60 °C in terms of pit size distribution.

Therefore, impedance spectra of a cylindrically shaped pit can be easily calculated in a way similar to the case of a cylindrically shaped pore if the impedance equation is expressed in an analytical form as follows [14]:

$$Z = (R_0 Z_0)^{1/2} \coth\left(l\sqrt{\frac{R_0}{Z_0}}\right) \tag{1}$$

where R_0 is the electrolyte resistance for a one-unit-length pit in $\Omega\ cm^{-1}$, Z_0 is the interfacial impedance for a one-unit-length pit in Ω cm and l is the pit length in cm. R_0 and Z_0 can be expressed as a function of the pit radius r as follows:

$$R_0 = \frac{\rho}{\pi r^2} \tag{2}$$

and:

$$Z_0 = \frac{Z_{eq}}{2\pi r} \tag{3}$$

where Z_{eq} is the interfacial impedance per surface unit in $\Omega\ cm^2$, and ρ the electrolyte resistivity in Ω cm. The combination of Eqs. 1, 2, 3 yields an expression for Z with respect to the two geometrical parameters l and r:

$$Z = \frac{(\rho Z_{eq})^{1/2}}{\sqrt{2}\pi r^{3/2}} \coth\left(l\sqrt{\frac{2\rho}{rZ_{eq}}}\right) \tag{4}$$

Because impedance spectra of the pitted specimen are caused by double-layer charging at the pit wall as well as charging at the pit bottom, it can be stated that the total impedance, Z_{total}, is represented by the summation of the impedance measured from all the pits.

For the sake of simplicity, it was assumed that the pit length is three times as long as the pit radius. In addition,

SEM observation showed that pit size distribution at 60 °C was divided into three classes, i.e. small-sized pits with an average pit radius of 48 μm, medium-sized pits with an average pit radius of 68 μm and large-sized pits with an average pit radius of 85 μm. In the cases at 100 °C and 150 °C, the pit size distribution was also divided into three classes like those at 60 °C. The pit size distribution can be easily calculated by the ratio of the number of pits with a certain size to the total pit number. The resulting pit size distribution of the three kinds of pits is listed as a function of solution temperature in Table 1.

The total impedance, Z_{total}, at 60 °C was analytically calculated from Eq. 4 by taking the value of the pit radius given above. Figure 3a and Fig. 3b show experimental impedance spectra in Nyquist presentation and plots at differential phase angles θ_d against frequency f, respectively, obtained from the pitted specimen prepared at 60 °C at open circuit potential in aqueous 0.5 M Na_2SO4 solution at room temperature, along with the simulated curves. The value of θ_d is defined as the angle of the slope of the Nyquist plot at a certain frequency. In Fig. 3b, it was noted that the values of θ_d were nearly constant over two frequency ranges, i.e. a lower constant value of θ_d (48°) in the higher frequency range and a higher constant value of θ_d (84°) in the lower frequency range. The former is due to the combination of the resistive element of the solution and the capacitive element at the pit wall, and at the same time the latter is attributed to double-layer charging at the pit bottom including prior double-layer charging at the pit wall.

Moreover, it should be noted that the first constant θ_d value of 48° was larger than the 45° in the higher frequency range and the second constant θ_d value of 84° was smaller than the 90° in the lower frequency range. It is well known [11, 15] that the impedance of a porous electrode in the absence of pore size distribution follows a linear line with a phase angle of 45° in the higher frequency range and then a vertical line in the lower frequency range in the Nyquist plot. Therefore, in the case of a cylindrically shaped pit it can be concluded that pit size distribution results in a deviation of θ_d from 45° and 90°, causing the occurrence of the inclined line in the Nyquist plot.

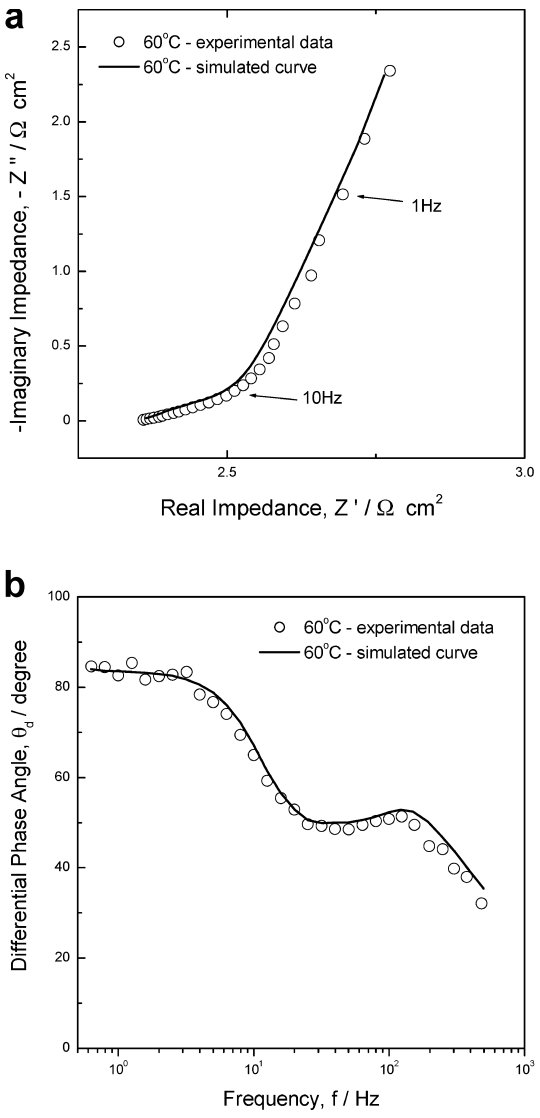

Fig. 3 a Impedance spectra in Nyquist presentation and **b** plots of differential phase angle θ_d vs. frequency f obtained from alloy 600 at open circuit potential in aqueous 0.5 M Na_2SO4 solution at room temperature after anodic polarization of 0.8 $V_{Ag/AgCI}$ for 300 s in aqueous 0.1 M $Na_2S_2O_3$ + 0.1 M NaCI solution at 60 °C. *Solid lines* represent the simulated impedance spectra

Analysis of impedance spectra of alloy 600 exposed to 100 °C and 150 °C solutions on the basis of the modified branched transmission line model

In the present work, the pitting process seems actually to proceed similarly to the generation process of the Koch construction [16], which represents the change in fractal geometry with time. The generation of the Koch construction first begins from a given geometry, i.e. the initiator, and then infinitely propagates with a broken line with sides of equal length, namely the generator. Instantaneous Koch construction and its generation process can thus describe well the many irregular shapes of pits and their formation and growth processes, respectively.

Figure 4 shows a schematic representation of the generation process of a triadic Koch construction with the fractal dimension $D_f = 1.26$. The triadic Koch construction begins with an equilateral triangle with sides of unit length. Then one pastes upon the mid-third of each side an equilateral triangle shaped peninsula with sides

Table 1 Pit size distribution of the three kinds of pit as a function of solutiontemperature. The distribution is given as fractions

	60 °C	100 °C	150 °C
A small-sized pit	0.44	0.30	0.24
A medium-sized pit	0.28	0.50	0.52
A large-sized pit	0.28	0.20	0.24

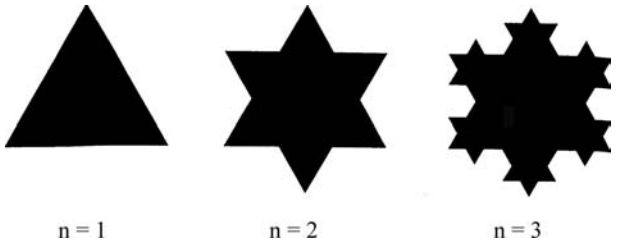

Fig. 4 Schematic representation of the generation process of the triadic Koch construction with a fractal dimension of 1.26. The initiator is an equilateral triangle with sides of unit length, the generator is an equilateral triangle-shaped peninsula with sides of length 1/3 and n represents the generation sequence of the Koch construction

of length 1/3. The same process of addition of peninsulas is repeated infinitely.

The value of the fractal dimension of the corrosion pits formed at 100 °C was determined to be 1.24 ± 0.06 and they actually grew in a way similar to the generation of the triadic Koch construction with $D_f = 1.26$, as shown in Fig. 4. For the sake of simplicity of simulation of the impedance spectra, it is assumed that $n = 1$, 2 and 3 in the three-dimensional triadic Koch constructions roughly correspond to a small-sized pit, a medium-sized pit and a large-sized pit, respectively. Since our previous work [8] showed that the pitting process reached a steady state and that the pit growth rate equaled the repassivation rate at 100 °C within 300 s, it is further assumed that the three-dimensional geometry of $n = 1$, 2 and 3 has the same aspect ratio (l/r ratio) as a small-sized pit, a medium-sized pit and a large-sized pit developed at 100 °C in 300 s, respectively.

On the basis of the observation of CPEs in the Nyquist plots and branched pit morphology, we propose a modified branched transmission line circuit for the triadic Koch construction, as shown in Fig. 5. The transmission line model is modified to simulate ion diffusion in the lateral direction as well as in the downward direction in a pit. Thus, the modified branched transmission line circuit is composed of a series combination of resistance and capacitance in the lateral and downward directions of the three-dimensional triadic Koch construction. The degree of branching in the lateral direction is determined to be proportional to the pit size and pit number density.

Under the circumstances, we first determined the resistive and capacitive elements of those three kinds of triadic constructions from the electrolyte resistance divided by their apparent area and double layer capacitance multiplied by their wall area, respectively, by taking the value of the area of those constructions. We next calculated the impedance spectra of the three kinds of triadic constructions during double-layer charging at the pit wall through the pit bottom using a simulation program with integrated circuit emphasis (SPICE) based upon a branched transmission line circuit in Fig. 5. The SPICE is a mathematical tool frequently used in electrical engineering to solve systems of equations characterizing a circuit. In contrast to the case of analytical

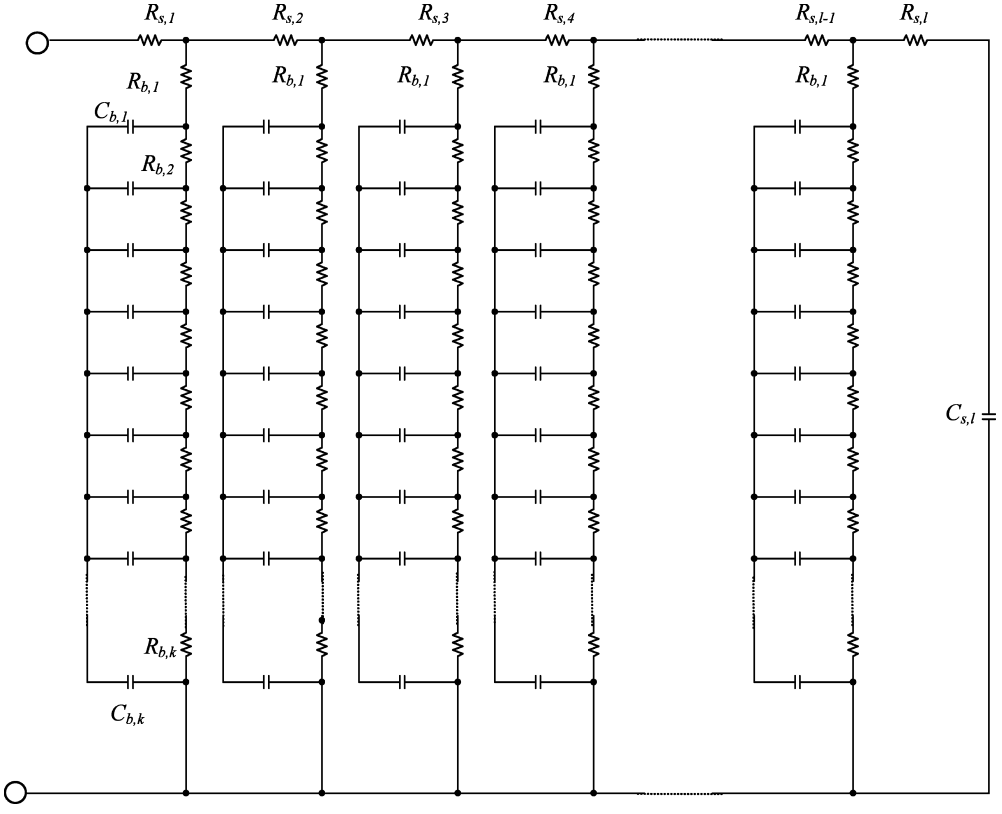

Fig. 5 A branched transmission line circuit of the triadic Koch construction. $R_{s,i}$ is the ith resistive element, $R_{b,i}$ is the ith resistive element in the branched area, $C_{s,i}$ is the ith capacitive element, $C_{b,i}$ is the ith capacitive element in the branched area and l is the number of transmission elements

simulation at 60 °C, we calculated the total impedance, Z_{total}, numerically by the summation of the impedance calculated from those three kinds of triadic constructions.

Figure 6a and Fig. 6b demonstrate experimental impedance spectra in Nyquist presentation and plots of θ_d against f obtained from the pitted specimen prepared at 100 °C at open circuit potential in aqueous 0.5 M Na_2SO4 solution at room temperature, along with the simulated curves. The simulated and experimental impedance spectra coincided well with each other over the frequency range of 10^3 to 1 Hz. It can be seen that the impedance spectra numerically simulated were similar to those spectra analytically calculated in the case of a cylindrically shaped pit formed at 60 °C in value and in shape.

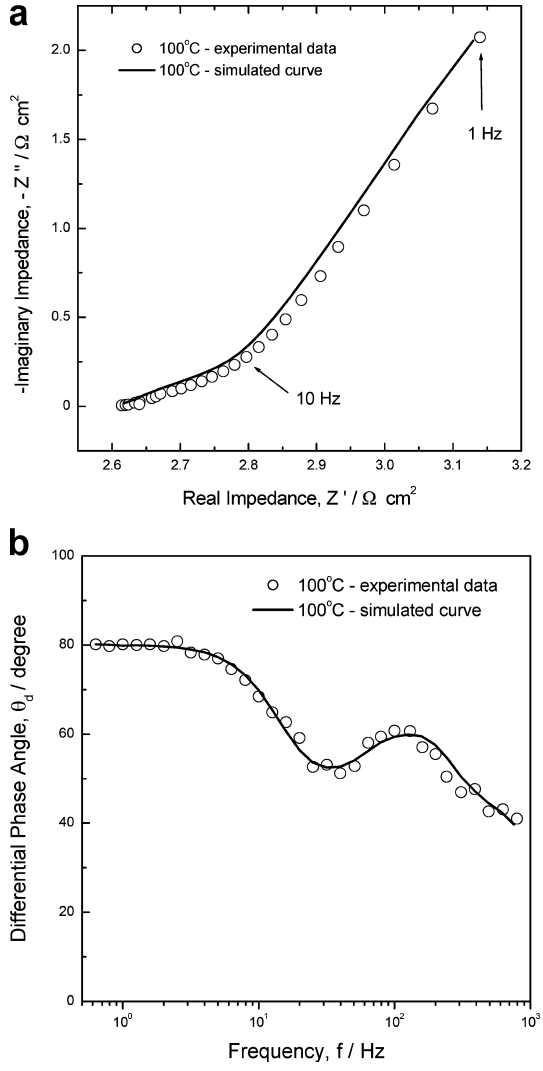

Fig. 6 **a** Impedance spectra in Nyquist presentation and **b** plots of differential phase angle θ_d vs. frequency f obtained from alloy 600 at open circuit potential in aqueous 0.5 M Na_2SO4 solution at room temperature after anodic polarization of 0.8 $V_{Ag/AgCI}$ for 300 s in aqueous 0.1 M $Na_2S_2O_3$ + 0.1 M NaCI solution at 100 °C. *Solid lines* represent the simulated impedance spectra

In a similar way, the pitting process of the specimen prepared at 150 °C can be described by the generation process of the quadratic Koch construction with $D_f = 1.5$, as given in Fig. 7. In this case, the quadratic Koch construction initiates with a square with sides of unit length and then propagates with repetitive protuberance and depression of a square with sides of length 1/4, and so on.

In the same manner as the simulation at 100 °C, we numerically calculated impedance spectra of the three kinds of quadratic Koch constructions for $n = 1$, 2 and 3 as given in Fig. 7 during double-layer charging at the pit wall to the pit bottom using a SPICE on the basis of the equivalent circuit given in Fig. 8. Figure 9a and Fig. 9b give experimental impedance spectra in Nyquist presentation and plots of θ_d against f obtained from the pitted specimen prepared at 150 °C at open circuit potential in aqueous 0.5 M Na_2SO4 solution at room temperature, along with the simulated curves.

From the results of Figs. 6 and 9, it is easily seen that the impedance spectra numerically calculated matched well those spectra experimentally measured over the frequency range of 10^3 to 1 Hz. This implies that pit size distribution as well as the value of the fractal dimension of the pits crucially influences the impedance spectra in value and in shape.

Now, it should be emphasized that impedance spectra analytically calculated based on the transmission line model at 60 °C were similar to those spectra numerically simulated based on the Koch constructions at 100 °C and 150 °C in value and in shape even though the value of the fractal dimension of the pits increased with increasing solution temperature. The value of the fractal dimension of the pits determined by the perimeter-area method was considerably influenced by the presence of even the small-sized pits and the medium-sized pits, since their pit sizes range between the inner cutoff length and the outer cutoff length satisfying the fractal geometry. It should be mentioned that in our previous work [8] the inner cutoff length and the outer cutoff length were estimated to be approximately 0.01 μm and 170 μm, respectively.

In contrast, the calculated impedance spectra were not significantly influenced by the small-sized pits and the medium-sized pits, but they were mainly influenced by the large-sized pits. In the case of the small-sized pits and the medium-sized pits, their pit sizes are not large

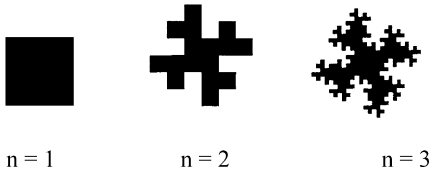

Fig. 7 Schematic representation of the generation process of the quadratic Koch construction with a fractal dimension of 1.5. The initiator is a square with sides of unit length, the generator is the protuberance and depression of a square with sides of length 1/4 and n represents the generation sequence of the Koch construction

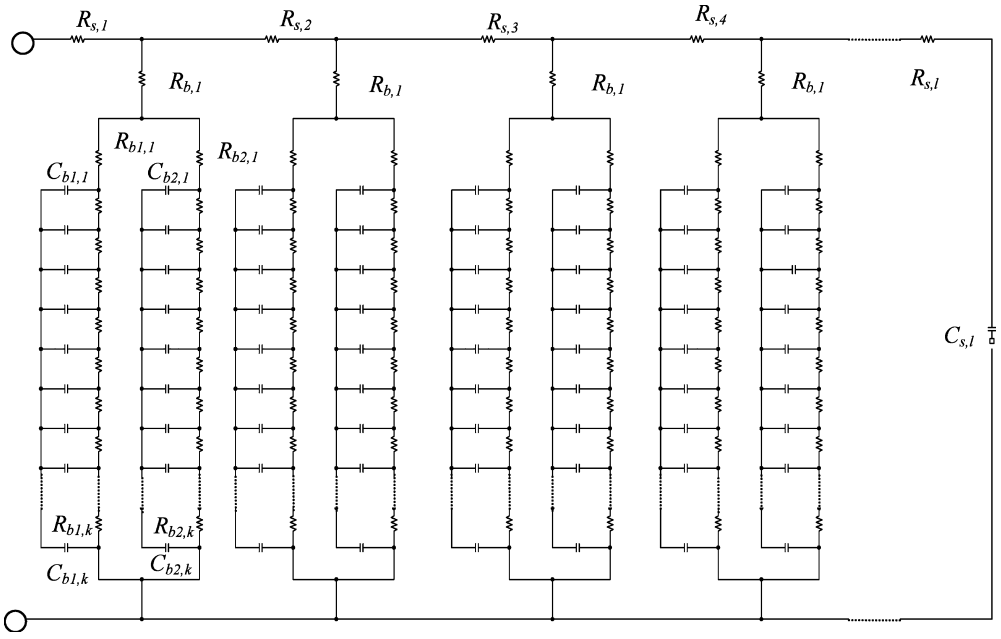

Fig. 8 A branched transmission line circuit of a quadratic Koch construction. $R_{b1,i}$ is the ith resistive element in the first branched area, $R_{b2,i}$ is the ith resistive element in the second branched area, $C_{b1,i}$ is the ith capacitive element in the first branched area, $C_{b2,i}$ is the ith capacitive element in the second branched area and I is the number of transmission elements

enough to sense the equipotential planes, which implies that their pit sizes are much smaller than the inner cutoff length of the equipotential planes. The inner cutoff and outer cutoff lengths are easily related to the outer cutoff and inner cutoff frequencies, respectively, through the product of the specific double-layer capacitance and the specific resistivity of the solution. The inner cutoff and outer cutoff frequencies are determined by the lowest and highest frequencies, respectively, at which CPE behaviour appears.

However, in the case of the large-sized pits, the equipotential planes are placed along the boundary of the pits, which means that the sizes of the large-sized pits just lie between the inner cutoff length and the outer cutoff length. Therefore, the calculated impedance spectra can sense the equipotential planes which are just established along the large-sized pits.

Consequently, the impedance of the large-sized pits mostly contributed to the total impedance, Z_{total}, of the pits experimentally measured and numerically calculated. As a result, the impedance spectra experimentally measured and numerically calculated from the three kinds of pitted specimens as a function of solution temperature were similar to one another in value and in shape.

Effect of surface roughness on impedance behaviour of alloy 600 exposed to solutions at 200–300 °C

Figure 10 presents impedance spectra in Nyquist presentation obtained from alloy 600 at an applied potential of 0.2 $V_{Ag/AgCl}$ in aqueous 0.1 M $Na_2S_2O_3 + 0.1$ M NaCl solution at various solution temperatures. In this figure, the size of the capacitive loop measured above 200 °C decreased markedly compared with that measured at 25 °C. This implies that increasing the solution temperature facilitated the formation of a non-protective oxide layer on the specimen, causing an intense corrosion phenomenon over the whole surface of the specimen.

It should be stressed that the Nyquist plots were found to be depressed more markedly from a perfect semicircular form with increasing solution temperature. The depression of the impedance spectra from a perfect semicircle is ascribed to the promotion of a surface roughening effect of the specimen. This can be validated by the decrease in the depression parameter and by the increase in surface roughness.

The impedance of a real electrode is frequently represented by an equivalent circuit containing a CPE showing power-law frequency dependence as follows [17]:

$$Z_{\text{CPE}} = \frac{1}{C}(j\omega)^{-p} \tag{5}$$

where C and p represent the capacitance and the depression parameter, respectively, and ω represents the angular frequency. Figure 11 demonstrates the applied potential dependence of the depression parameter determined from the Nyquist plots obtained from the specimen in aqueous 0.1 M $Na_2S_2O_3 + 0.1$ M NaCl solution at various solution temperatures. The value of the depression parameter diminished with increasing solution temperature. Considering that a major cause of depression of the impedance spectra is known to be of geometric origin, it is inferred that depression of the impedance spectra of the pitted specimen stems from an increase in the surface roughness of the specimen.

In our previous work [8] it was observed from SEM micrographs that the morphology of the pits changed from a highly branched shape in the early stage of the pitting process to a widely grooved shape in the later stage, owing to the lower degree of passivity of the oxide

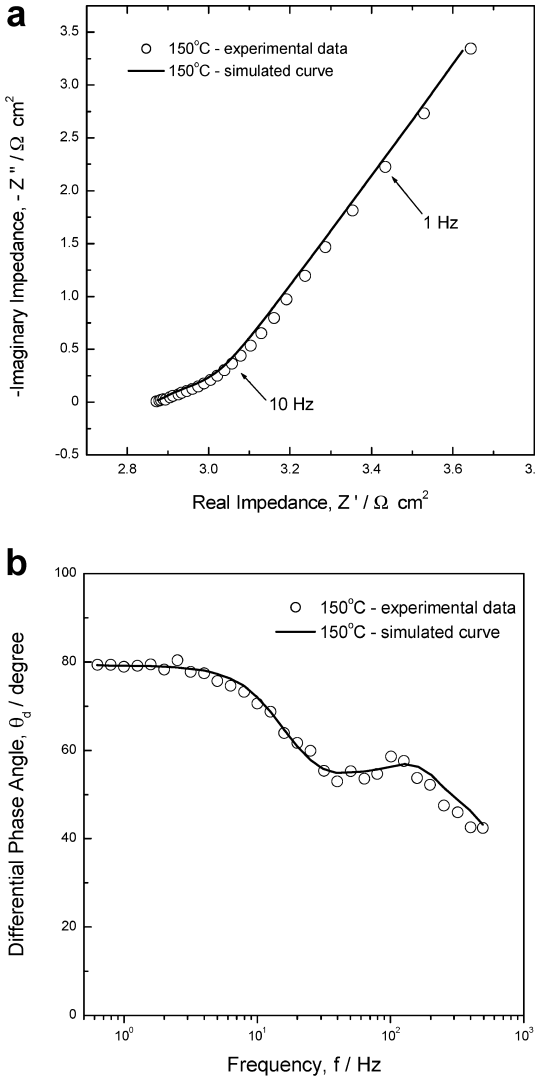

Fig. 9 **a** Impedance spectra in Nyquist presentation and **b** plots of differential phase angle θ_d vs. frequency f obtained from alloy 600 at open circuit potential in aqueous 0.5 M Na_2SO4 solution at room temperature after anodic polarization of 0.8 $V_{Ag/AgCl}$ for 300 s in aqueous 0.1 M $Na_2S_2O_3 + 0.1$ M NaCl solution at 150 °C. *Solid lines* represent the simulated impedance spectra

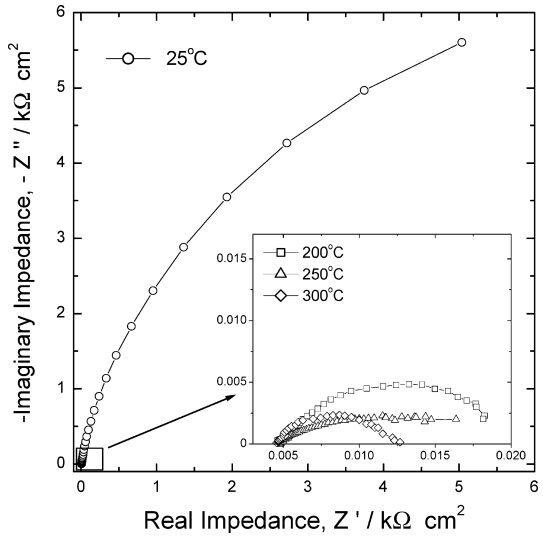

Fig. 10 Impedance spectra in Nyquist presentation obtained from alloy 600 at an applied potential of 0.2 $V_{Ag/AgCl}$ in aqueous 0.1 M $Na_2S_2O_3 + 0.1$ M NaCl solution at various solution temperatures

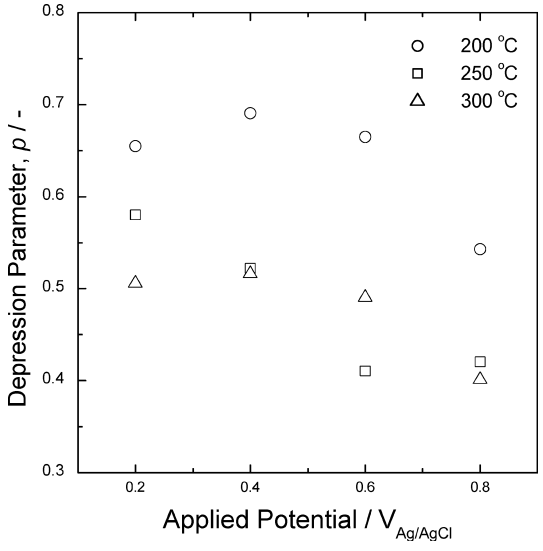

Fig. 11 Changes in the depression parameter p with applied anodic potential obtained from alloy 600 in aqueous 0.1 M $Na_2S_2O_3 + 0.1$ M NaCl solution at various solution temperatures

film above 200 °C. Moreover, the transition in morphology from a highly branched shape to a widely grooved shape occurred more markedly with increasing solution temperature. Hence it is conceivable that the surface roughness also increased with increasing solution temperature.

In this work, the increase in the surface roughness with solution temperature was experimentally verified by analysis of the AFM images. For the analysis of an AFM image, the root-mean-square roughness, R_{rms}, was introduced as an indirect measure of the surface roughness of the specimen. It was found that the value of R_{rms} increased with increasing solution temperature as follows: $R_{rms}(200\ °C) = 0.49\ \mu m$, $R_{rms}(250\ °C) = 0.67\ \mu m$ and $R_{rms}(300\ °C) = 0.84\ \mu m$. Consequently, it can be concluded that the depression of the impedance spectra above 200 °C comes from an increase in the surface roughness of the specimen by the formation and further growth of the pits.

Conclusions

The following summary may be given:

1. Impedance spectra of pitted alloy 600 electrodes exposed to solutions at 60–150 °C revealed that they were divided into two sections with different values for the slope. The first CPE with a smaller slope in the frequency range from 10^3 to 10 Hz results from a

combination of the resistive element of the solution and the capacitive element at the pit wall. Subsequently, the second CPE with a larger slope in the frequency range from 10 to 1 Hz is attributed to double-layer charging at the pit bottom, including prior double-layer charging at the pit wall.

2. At 60 °C, the transmission line model based upon a cylindrically shaped pit was employed to analyse the impedance spectra of the pitted electrode with regard to the pit size distribution. Pit size distribution is categorized by three classes, i.e. small-, medium- and large-sized pits with average pit radii of 48, 68 and 85 μm, respectively. As a result, the size distribution of pits with a cylindrical shape considerably affects double-layer charging at the pit wall as well as charging at the pit bottom, leading to the inclined line in the Nyquist plot.
3. At 100 °C and 150 °C, impedance spectra were calculated numerically, based upon the modified branched transmission line circuit by taking into account the pit size and the fractal dimension of the pits. As a model system, the triadic and quadratic Koch constructions whose fractal dimension values are 1.26 and 1.5, respectively, were employed to simulate the impedance spectra containing a CPE. The impedance spectra numerically calculated matched well those spectra experimentally measured over the frequency range of 10^3 to 1 Hz.
4. Above 200 °C, the depression of the impedance spectra is caused by roughening of the electrode surface resulting from acceleration of the formation and growth of the pits due to a decrease in the degree of passivity of the oxide film.

Acknowledgements This work was partly supported by the Brain Korea 21 project. The authors are indebted to Mr. S.-B. Lee, Corrosion and Interfacial Electrochemistry Research Laboratory, Korea Advanced Institute of Science Technology, for helpful discussions.

References

1. Karaminezhaad-Rajbar M, Mankowski J, Macdonald DD (1985) Corrosion 41:197
2. Park JR, Szklarska-Smialowska Z (1985) Corrosion 41:665
3. Rajan VB, Was GS (1987) Corrosion 43:305
4. Frankel GS (1990) Corros Sci 30:1203
5. Costa JM, Sagues F, Vilarrasa M (1991) Corros Sci 32:665
6. Holten T, Jøssang T, Meakin P, Feder J (1994) Phys Rev E 50:754
7. Balazs L, Gouyet JF (1995) Physica A 217:319
8. Park JJ, Pyun SI (2003) Corros Sci (in press)
9. Mandelbrot BB, Passoja DE, Paullay AJ (1984) Nature 308:721
10. Feder J (1988) Fractals. Plenum, New York, p 200
11. Song HK, Jung YH, Lee KH, Dao Le H (1999) Electrochim Acta 44:3513
12. de Levie R (1964) Electrochim Acta 9:1231
13. de Levie R (1967) In: Delahay P (ed) Advances in electrochemistry and electrochemical engineering, vol. 6. Interscience, New York, p
14. Los P, Lasia A, Ménard H, Brossard L (1993) J Electroanal Chem 360:101
15. Keiser H, Beccu KD, Gutjahr MA (1976) Electrochim Acta 21:539
16. Mandelbrot BB (1983) The fractal geometry of nature. Freeman, New York, p 50
17. Macdonald JR (1987) Impedance spectroscopy. Wiley, New York, p 17